

RESEARCH ARTICLE | JULY 05 2023

## Versatile and robust reconstruction of extreme-ultraviolet pulses down to the attosecond regime <sup>EP</sup>

Gian Luca Dolso <sup>ID</sup>; Giacomo Inzani <sup>ID</sup>; Nicola Di Palo <sup>✉</sup> <sup>ID</sup>; Bruno Moio <sup>ID</sup>; Fabio Medeghini; Rocio Borrego-Varillas <sup>ID</sup>; Mauro Nisoli <sup>ID</sup>; Matteo Lucchini <sup>ID</sup>

 Check for updates


APL Photonics 8, 076101 (2023)

<https://doi.org/10.1063/5.0145325>

  
View  
Online

  
Export  
Citation

CrossMark



THE ADVANCED MATERIALS MANUFACTURER®

yttrium iron garnet    glassy carbon    beamsplitters    fused quartz    additive manufacturing

zeolites    III-IV semiconductors    gallium lump    copper nanoparticles    organometallics

nano ribbons    barium fluoride    europium phosphors    photonics    infrared dyes

sapphire windows    Nd:YAG    epitaxial crystal growth    ultra high purity materials    transparent ceramics    CIGS

spintronics    raman substrates    cerium oxide polishing powder    cermet    nanodispersions

silver nanoparticles    perovskites    surface functionalized nanoparticles    MBE grade materials    thin film

MOCVD    beta-barium borate    K Ca Sc Ti V Cr Mn Fe Co Ni Cu Zn Ga Ge As Se Br Kr    OLED lighting    solar energy

rare earth metals    quantum dots    Rb Sr Y Zr Nb Mo Tc Ru Rh Pd Ag Cd In Sn Sb Te I Xe    sputtering targets    fiber optics

osmium    scintillation Ce:YAG    Cs Ba La Hf Ta W Re Os Ir Pt Au Hg Tl Pb Bi Po At Rn    h-BN    deposition slugs


refractory metals    laser crystals    Fr Ra Ac Rf Db Sg Bh Hs Mt Dst Rg Cn Nh Fl Mo Lv Ts Og    CVD precursors    photovoltaics

anodic aluminum oxide    niobate    InAs wafers    Ce Pr Nd Pm Sm Eu Gd Tb Dy Ho Er Tm Yb Lu    metamaterials    borosilicate glass

ZnS    CdTe    MOFs    AuNPs    Th Pa U Np Pu Am Cm Bk Cf Es Fm Md No Lr    YBCO    superconductors    InGaAs

perovskite crystals    transparent ceramics    indium tin oxide    MgF2    rutile    optical glass

diamond micropowder



**Now Invent.™**

[www.americanelements.com](http://www.americanelements.com)

© 2001-2022, American Elements LLC, a U.S. Registered Trademark.

The Next Generation of Material Science Catalogs

# Versatile and robust reconstruction of extreme-ultraviolet pulses down to the attosecond regime

Cite as: APL Photon. 8, 076101 (2023); doi: 10.1063/5.0145325

Submitted: 5 February 2023 • Accepted: 13 June 2023 •

Published Online: 5 July 2023



View Online



Export Citation



CrossMark

Gian Luca Dolso,<sup>1</sup>  Giacomo Inzani,<sup>1</sup>  Nicola Di Palo,<sup>1,a)</sup>  Bruno Moio,<sup>1</sup>  Fabio Medeghini,<sup>1</sup>   
Rocío Borrego-Varillas,<sup>2</sup>  Mauro Nisoli,<sup>1,2</sup>  and Matteo Lucchini<sup>1,2</sup> 

## AFFILIATIONS

<sup>1</sup>Department of Physics, Politecnico di Milano, 20133 Milano, Italy

<sup>2</sup>Institute for Photonics and Nanotechnologies, IFN-CNR, 20133 Milano, Italy

<sup>a)</sup>Author to whom correspondence should be addressed: [nicola.dipalo@polimi.it](mailto:nicola.dipalo@polimi.it)

## ABSTRACT

A reliable and complete temporal characterization of ultrashort pulses is a crucial requisite for the correct interpretation of time-resolved experiments. This task is particularly challenging in the extreme-ultraviolet (XUV) spectral region, where usually different approaches are employed depending on the exact temporal structure of the pulses. Here we propose and validate against both simulated and experimental data a novel approach for the reconstruction of ultrashort XUV pulses produced by high-order harmonic generation in gases for three different conditions: isolated attosecond pulses, attosecond pulse trains, and few-femtosecond pulses obtained by spectral selection of single harmonics. The core of the method, named simplified trace reconstruction in the perturbative regime (STRIFE), is a novel mathematical description providing a simplified picture of the two-color photoionization process. This new approach is capable of accurately retrieving the temporal characteristics of the XUV pulses with notably reduced computational costs compared to other currently used reconstruction techniques. Direct comparison to standard approaches proves it to be superior in terms of flexibility, reliability, and robustness against noise and acquisition artifacts, making STRIFE a promising tool for pulse characterization.

© 2023 Author(s). All article content, except where otherwise noted, is licensed under a Creative Commons Attribution (CC BY) license (<http://creativecommons.org/licenses/by/4.0/>). <https://doi.org/10.1063/5.0145325>

## I. INTRODUCTION

Extreme-ultraviolet (XUV) pulses with ultrashort duration, down to the attosecond regime, are unique tools capable of accessing electronic and nuclear dynamics in atoms, molecules, and solids.<sup>1,2</sup> A crucial prerequisite for a detailed analysis of time-resolved measurements is a precise knowledge of the temporal characteristics of the pulses employed in the experiments. As a matter of fact, the development of complete and robust characterization methods has been one of the primary objectives of attosecond science. At first, to prove the generation of attosecond pulses, and later, to allow a correct interpretation of spectroscopic data and explore the true limits of attosecond time-resolved techniques in the matter.<sup>3–16</sup>

Ultrashort XUV pulses are usually produced by means of high-order harmonic generation (HHG), in which intense infrared (IR) driving pulses are focused on noble gases. Depending on the

duration of the IR pulses and on the experimental setup, isolated attosecond pulses (IAPs), attosecond pulse trains (APT), or few-femtosecond XUV pulses obtained by spectral selection of single harmonics (SHs) can be generated.<sup>2</sup> Despite their quite different properties, the temporal characterization of these pulses can be retrieved by performing two-color (IR/XUV) photoemission experiments on atomic targets, employing the so-called attosecond streak-camera approach.<sup>17</sup> In this method, the spectral amplitude of the photoemitted electrons is directly measured as a function of the relative delay between XUV and IR pulses. The spectral phase is then reconstructed from the measured spectrogram by employing iterative algorithms, using an approach similar to the frequency-resolved optical gating (FROG) technique<sup>18</sup> employed in the case of visible/infrared femtosecond pulses. The temporal properties of both XUV and IR pulses can be fully characterized since they determine the final photoelectron spectrum.

Over the years, considerable effort has been invested in improving reconstruction in terms of robustness against experimental non-idealities,<sup>19,20</sup> applicability range,<sup>21</sup> and accuracy.<sup>22–27</sup> However, a versatile, reliable, and fast method applicable to ultrashort XUV pulses irrespective of their temporal structure (i.e., IAPs, APTs, or few-femtosecond XUV pulses) and robust against typical experimental difficulties (noise, detection artifacts) is still lacking. While the characterization of IAPs from a two-color photoelectron spectrogram is nowadays well established and can also count on alternative approaches,<sup>28–31</sup> the reconstruction in the case of APTs and SHs is more critical. In this latter case, for example, the narrower bandwidth of the XUV radiation, the lost sub-cycle resolution, and the absence of sensitive interference structures challenge standard reconstruction techniques, which may fail if proper data optimization is not performed prior to reconstruction.<sup>32</sup> As a result, a proper characterization of the most advanced light sources, such as x-ray free-electron lasers, is not always possible.<sup>33</sup> Bucking the present trend, which increases the reconstruction complexity by including additional effects like angular averaging,<sup>34</sup> partial coherence,<sup>35</sup> and the target dipole,<sup>36</sup> in this work we introduce a conceptually novel approach that simplifies the treatment. Due to the less complex mathematical form, the spectrogram can be reconstructed through a non-linear fitting procedure based on a semi-analytical expression for the involved IR and XUV electric fields, allowing for the use of a significantly reduced set of fit parameters. This increases the versatility, allowing for the inclusion of additional information on the experimental parameters in the retrieval, ultimately enhancing the accuracy of the reconstruction and the robustness against experimental imperfections.

The method, named simplified trace reconstruction in the perturbative regime (STRIFE), is first validated against simulations, proving its applicability to extreme cases that cannot be treated with standard approaches. STRIFE is then applied to experimental photoelectron spectrograms generated by IAPs, APTs, and few-fs SHs. Thanks to the possibility of considering independent measurements of the radiation photon spectra and the acquisition system instrumental response function (IRF), a detailed comparison with standard ptychographic reconstruction<sup>37</sup> proves STRIFE to be superior in terms of computational costs and consistency of the results. Additionally, STRIFE can be naturally applied to differential spectrograms obtained by subtracting from the pump-probe trace the XUV-only photoelectron spectrum measured at each delay to achieve higher robustness against noise. We note that while this solution might be adopted with other existing methods, it is not for granted that blind-FROG approaches will converge when constrained to work on differential spectrograms with fixed spectral amplitudes. Our results, thus, prove STRIFE to be particularly powerful when dealing with non-ideal traces, realizing a key prerequisite for the correct development of extreme time-resolved spectroscopy.

## II. MATHEMATICAL MODEL

The most commonly used techniques for the reconstruction of attosecond pulses are based on the attosecond streak camera principle,<sup>17</sup> for which a schematic is reported in Fig. 1(a). The attosecond radiation, typically in the XUV, ionizes an atomic target away from resonances so that the photoemitted electron wavepacket can be considered a temporal copy of the ionizing pulses.<sup>38</sup> An

intense IR pulse ( $I_{IR} \sim 10^{10} - 10^{12}$  W/cm<sup>2</sup>) acts as a phase modulator changing the photoelectron spectrum, which is collected by a spectrometer [typically a time-of-flight (TOF) spectrometer]. Within the strong field approximation, the photoelectron spectrum is given by the Fourier transform of the scattering amplitude between the initial atomic bound state and the final state of the electron, approximated with a Volkov wave.<sup>39,40</sup>

The resulting collection of photoelectron spectra as a function of the electron final energy  $\hbar\omega$  and the relative delay  $\tau$  between the pulses (hereafter spectrogram) can be written as (atomic units are used),<sup>41</sup>

$$S(\omega, \tau) = \left| \int_{-\infty}^{\infty} E_x(t - \tau) e^{-i\varphi(t,p)} e^{i(I_p + \omega)t} dt \right|^2, \quad (1)$$

where the atomic dipole that describes XUV photoionization is assumed to be constant within the energy region of interest.  $E_x(t)$  is the XUV electric field,  $I_p$  is the target ionization potential, and  $\omega$  is the electron kinetic energy, connected to the particle's final momentum  $p$  by the relation  $\omega = p^2/2$ . The phase term

$$\varphi(t, p) = \int_t^{\infty} \left[ pA(t') + \frac{1}{2}A^2(t') \right] dt', \quad (2)$$

often called the quantum phase, describes the interaction between the IR vector potential,  $A(t)$ , and the photoelectron in the continuum. The above-mentioned equations hold within the framework of the Strong Field Approximation (SFA) and, therefore, neglect Coulomb effects, which may, however, become relevant at photon energies close to the ionization potential of the target. A spectrogram simulated with Eq. (1) for chirped XUV and IR pulses with transform-limited full-width at half-maximum (FWHM) durations of 350 as and 5 fs, respectively, is presented in Fig. 1(b). As a result of the interaction,  $S(\omega, \tau)$  depends on both the temporal properties of the IR and XUV, allowing for their reconstruction through iterative algorithms, usually based on an approximated version of Eq. (1). The most commonly used approximation is the so-called central momentum approximation (CMA), for which the final electron momentum  $p$  in Eq. (2) is substituted with its central value  $p_c$ . This allows  $S(\omega, \tau)$  to be written as the Fourier transform of the product between two functions of time, one depending solely on the XUV field and the other on the IR,

$$S(\omega, \tau) \simeq \left| \int_{-\infty}^{\infty} E_x(t - \tau) e^{-i\varphi(t,p_c)} e^{i(I_p + \omega)t} dt \right|^2, \quad (3)$$

which can be treated in a FROG-like approach<sup>18</sup> using standard iterative algorithms.<sup>37,42,43</sup> If  $\varphi$  does not vary significantly within the energy region of interest, which is usually true when the photoelectron central kinetic energy is much larger than its bandwidth, the CMA does not introduce a large error [Fig. 1(c)]. It is worth noticing that this is the assumption upon which the large majority of the known reconstruction algorithms are based, and it does not represent a limitation specific to STRIFE. Keathley and co-workers have shown that the CMA can be relaxed in blind FROG methods at considerable additional computational costs.<sup>23</sup> We foresee that STRIFE could be extended in a similar fashion to avoid CMA, but its investigation goes beyond the scope of this work. Here, we

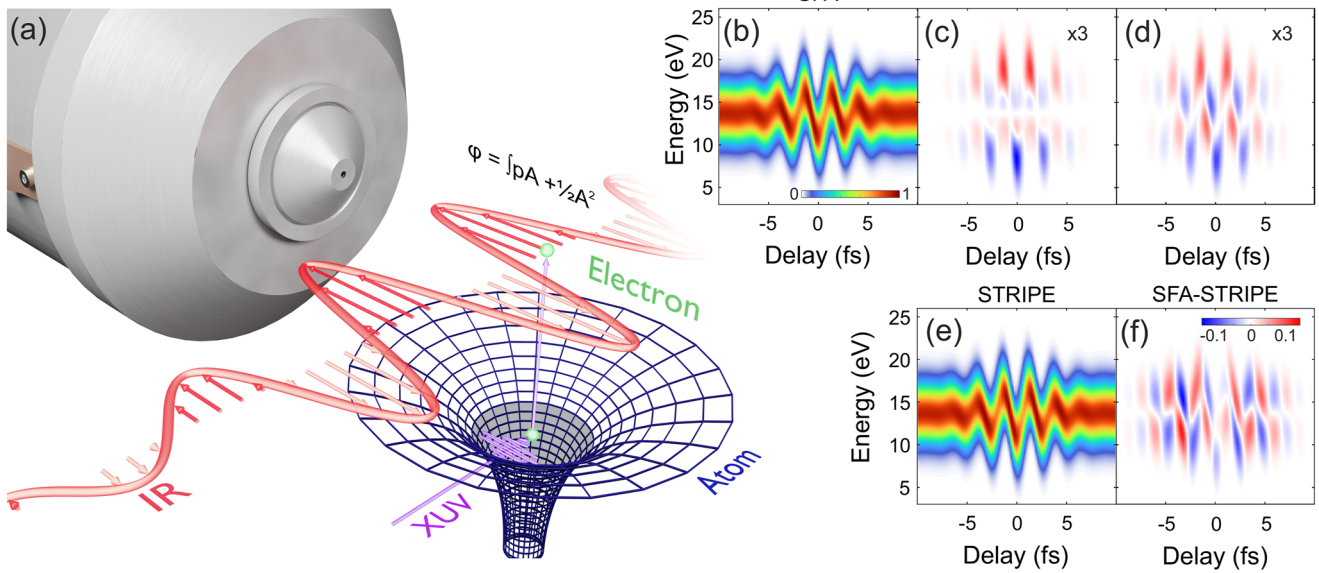


**FIG. 1.** (a) Schematic of the two-color ionization process where the emitted electron acquires a phase  $\varphi = \int_t^\infty [pA + \frac{1}{2}A^2] dt'$ . (b) and (e) Streaking spectrogram computed with the strong-field-approximation (SFA) formula, Eq. (1), or the STRIPE model, Eq. (4), respectively. (c), (d), and (f) Difference between the SFA calculations, which consider the full quantum phase  $\varphi$ , and computations with an increasing number of approximations: introducing the CMA, (c), neglecting  $A^2$ , (d), and the SVEA (STRIPE model), (f). Relevant parameters used in the simulations: XUV and IR transform limited time durations: 350 as and 5 fs. GDD on the XUV: 0.02 fs<sup>2</sup>, on the IR: 1 fs<sup>2</sup>. IR intensity:  $5 \times 10^{11}$  W/cm<sup>2</sup>. IR central wavelength 810 nm, XUV central energy  $\sim 35$  eV. Photoelectrons are produced by the ionization of Neon atoms.

follow the opposite approach and simplify the mathematical treatment of  $S(\omega, \tau)$  to obtain a versatile, quick, and yet reliable reconstruction. Starting from Eq. (3), we follow a perturbative approach<sup>44</sup> and neglect the  $A^2$  term in Eq. (2). If the field is not too strong (around  $10^{11}$  W/cm<sup>2</sup>), the error introduced is smaller than the one coming from the CMA [Fig. 1(d)]. Finally, if the IR envelope varies slowly in time (slowly-varying envelope approximation, SVEA),<sup>44</sup> the spectrogram can be rewritten in the form

$$S(\omega, \tau) \simeq \left| \int_{-\infty}^{\infty} E_x(t - \tau) e^{i\frac{p_x}{\omega_0} E(t)} e^{i(I_p + \omega)t} dt \right|^2, \quad (4)$$

where  $E(t) = -\frac{dA(t)}{dt}$  is the IR electric field and  $\omega_0$  is its central frequency.

The streaking trace simulated with Eq. (4) and for the same parameters as in Fig. 1(b) is displayed in Fig. 1(e). Despite being an extreme case, which uses a relatively strong ( $I_{IR} = 5 \times 10^{11}$  W/cm<sup>2</sup>) and short (roughly 5 fs) IR pulse and an XUV pulse with low central energy, certainly challenging CMA, SVEA, and the perturbative approximation, all the relevant features of the spectrogram are reproduced, and the error with respect to Eq. (1) stays below 14% [Fig. 1(f)]. To provide a more precise estimate of the error produced at each step of approximation, we computed the difference between the spectrogram produced with the SFA model and the trace obtained with an increasing number of approximations for the considered choice of XUV and IR pulses [see Figs. 1(c), 1(d),

and 1(f)]. In particular, we calculated the root mean square (rms) error associated with Fig. 1(c) (CMA), Fig. 1(d) (CMA+perturbative regime), and Fig. 1(f) (CMA+perturbative regime+SVEA), which amounts to  $5.7 \times 10^{-6}$ ,  $6.1 \times 10^{-6}$ , and  $1.1 \times 10^{-4}$ , respectively. For the chosen set of parameters, while removing the  $A^2$  term produces a negligible effect (rms error  $\sim 10^{-7}$ ), the largest error comes from the use of the SVEA approximation for a two-optical-cycle IR pulse. Noteworthy, the calculated rms errors are orders of magnitude lower than typical errors obtained for the reconstruction of noisy experimental data, usually in the  $10^{-2}$ – $10^{-3}$  range.

The error introduced because of the above-mentioned approximations strongly depends on the IR pulse duration and peak intensity. Figure 2 shows the evolution of the rms error for the simulation parameters of Fig. 1(b) when the IR duration or peak intensity is changed. We observe that the rms error increases by less than a factor two also for sub-2-cycle pulse durations (<5.32 fs) and that an intensity increment of an order of magnitude is needed to obtain a comparable error increment for 6.7 fs pulses. This shows that with longer and weaker IR pulses, the additional error introduced by the approximations becomes negligible, and Eq. (4) provides a simple description of the photoelectron spectrogram that can be used to develop a versatile non-linear fitting procedure capable of reconstructing the temporal properties of the IR and XUV pulses. This is the core idea at the basis of STRIPE, which we will show to offer significant advantages in terms of computational speed and convergence, especially with a noisy and imperfect acquisition scheme.

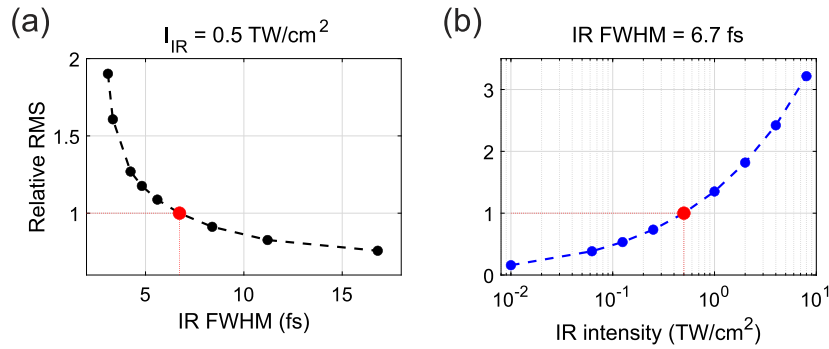


**FIG. 2.** Quantitative analysis of the error introduced by STRIPE as a function of IR pulse duration (a) and intensity (b). The red dots correspond to the values used for the simulation presented in Fig. 1(b) of the manuscript. In (a), the IR intensity is fixed and equal to  $5 \times 10^{11} \text{ W/cm}^2$ , while the duration in (b) is set to 6.7 fs.

### III. ALGORITHM DESCRIPTION

The simplified theoretical model described by Eq. (4) lies at the heart of the STRIPE algorithm. In particular, the entire STRIPE reconstruction is performed in MATLAB on a standard personal computer and uses a 2D non-linear least squares optimization procedure based on the trust region reflective algorithm as implemented in the standard MATLAB curve fitting toolbox. The fit procedure minimizes the difference between the experimental spectrogram and the one produced with Eq. (4) as a function of the IR and XUV complex electric fields, where the initial guesses for the pulses are defined in the spectral domain. The IR pulse is written in the form of a product between the modulus of the pulse spectrum,  $E_0(\omega)$ , and a polynomial phase,

$$\hat{E}(\omega) = E_0(\omega) \exp \left[ i \sum_{n=2}^N \frac{D^{(n)}}{n!} (\omega - \omega_0)^n \right]. \quad (5)$$

In its more general implementation, both the parameters that describe the analytical form of  $E_0(\omega)$  and the coefficients  $D^{(n)}$  are fitting parameters in the retrieval. Since Eq. (5) is not suited to describe the spectral behavior of an APT, which is not an even function of time, the XUV spectrum is instead written as the sum of two delayed contributions,

$$\hat{E}_x(\omega) = A(\omega)e^{i\phi(\omega)} + \alpha A(\omega)e^{i\phi'(\omega) + i\omega\tau}, \quad (6)$$

where the scalar  $\alpha$  is a free parameter of the fit,  $\phi(\omega)$  and  $\phi'(\omega)$  are two energy dependent phases of the form in Eq. (5), and the real amplitude  $A(\omega)$  is related to the XUV spectrum  $\hat{E}_x(\omega)$  by

$$A(\omega) = \frac{|\hat{E}_x(\omega)|}{\sqrt{1 + \alpha^2 + 2\alpha \cos(\phi' - \phi + \omega\tau)}}. \quad (7)$$

This allows fitting complex phase profiles, which can be present, for example, in the case of a main XUV pulse followed by a delayed satellite, without adding too many terms in the Fourier or Taylor expansion of the phase. Please note that the term  $A(\omega)$  does not necessarily represent an individual pulse; in the case of APT, for example, it describes a train of pulses in time.

For all the reconstructions presented in this work, the set of functions used to describe both pulses is the following: the IR pulse

is described by a Gaussian envelope, which multiplies a fourth-order polynomial phase term. The XUV pulse is described by two delayed contributions, as indicated in Eq. (6), where the amplitude spectrum is always kept fixed as a constraint while the fit routine reconstructs the two phase terms, each one described by a third-order expansion. This specific choice turned out to successfully model all the pairs of XUV and IR pulses investigated in our study. We note that since both the IR and XUV spectral intensities can be set to the experimental ones, the choice of the fitting function used to describe the radiation becomes less critical as it is limited to a correct description of the pulse spectral phases, often achieved with a polynomial. While independent knowledge of the radiation spectra surely assures faster and more accurate reconstruction, STRIPE can also run without this information. In such a case, the spectral amplitudes need to be properly modeled with a sum of analytical functions, increasing the number of fit parameters to be retrieved. We found this procedure to give comparable results, provided that an educated guess of the spectral shape of the pulses can be performed.

It is worth noting that there exists another reconstruction algorithm, called Phase Retrieval by Omega Oscillation Filtering (PROOF),<sup>45</sup> which assumes the XUV spectral amplitude to be known and retrieves only its spectral phase in the perturbative regime. While PROOF does not need to assume any specific functional form for the XUV phase, it is normally employed for the reconstruction of IAPs and does not allow retrieving the IR temporal profile. Although this technique has been recently improved to include processes described in second-order perturbation theory,<sup>46,47</sup> the perturbative approximation performed in PROOF is more severe than the one at the core of STRIPE, possibly limiting its applicability.

The simplified theoretical description of the physics underlying two-color photoionization allows for a versatile and fast retrieval of the involved IR and XUV pulses due to the small set of parameters that can be employed to describe the physical process within the discussed approximations. The achieved theoretical compactness translates into the possibility of including within the fitting procedure any additional information that may be known experimentally, with the goal of enhancing the robustness and accuracy of the retrieval. Such information, as discussed in the following, may include the measured spectra of the IR and XUV pulses, the IR-off photoelectron spectrum, and the instrumental response function of the electron detection system.

IV. ALGORITHM VALIDATION

In order to validate STRIPE, we first tested the algorithm on simulated traces and compared its results with the output of a standard algorithm like the extended Ptychographic Iterative Engine (ePIE).<sup>37</sup> At first, we applied our method to ideal traces, and later we investigated its performance with noisy traces and in the case of distorted traces, e.g., due to a finite instrumental response function (IRF) of the acquisition system.

A. Reconstruction of simulated traces

The left side of the first column in Figs. 3(a), 3(d), and 3(g) (left side) shows the spectrograms simulated in neon with the strong field approximation (SFA) formula of Eq. (1) for an SH (top row), an APT (middle row), and an IAP (bottom row) [Figs. 3(b), 3(e), and 3(h)]. The initial XUV [Figs. 3(b), 3(e), and 3(h)] pulses used to simulate the spectrograms are reported in the last two columns on the right with solid gray curves. For the SH and APT, the IR has an intensity FWHM duration of 16 fs and a peak intensity  $I_{IR} = 1 \times 10^{11}$  W/cm<sup>2</sup>. In the IAP case, the IR lasts for  $\sim 6.7$  fs, and  $I_{IR} = 5 \times 10^{11}$  W/cm<sup>2</sup>. The STRIPE reconstructed spectrograms are displayed in the right panels of the first column of Figs. 3(a), 3(d), and 3(g) (right side), while the retrieved pulses are marked in the last two columns by the red dashed curves. In the same panels, the blue dotted curves are the result of an ePIE reconstruction. To estimate the

consistency of the obtained results, we run several STRIPE retrievals for each spectrogram with 100 different initial guesses, reporting error bars corresponding to twice the standard deviation over the whole set of reconstructions.

We found STRIPE to correctly reconstruct both the IR and the XUV radiation in all the cases, with accuracy comparable to the one given by ePIE (compare the blue and red error bars), but with considerably increased reconstruction speed. While ePIE requires about 10 min to converge on a personal computer for a 1500 (energy)  $\times$  250 (delay) point dataset, STRIPE reconstructions of equivalent resolution are obtained in  $\leq 1$  min. The time needed to reach fit convergence with STRIPE is mainly dependent on the size of the data matrix to reconstruct. We found no significant change in reconstruction speed for the reported datasets of similar size.

Interestingly, the results are accurate also for the spectrogram generated by an IAP (bottom row in Fig. 3), where the CMA is stressed by the broad XUV bandwidth, while the perturbative regime and the SVEA are challenged by the intense and short IR pulse. However, it is worth noticing that the STRIPE reconstruction error appears to increase by a factor of 10 between the IAP and the APT [compare the red error bars in Figs. 3(h) and 3(e)]. This is due to the increased complexity of the spectrogram and the increasing number of non-trivial features that must be fitted. The same trend (increasing error) is observed for ePIE [compare the blue error bars in Figs. 3(h) and 3(e)].

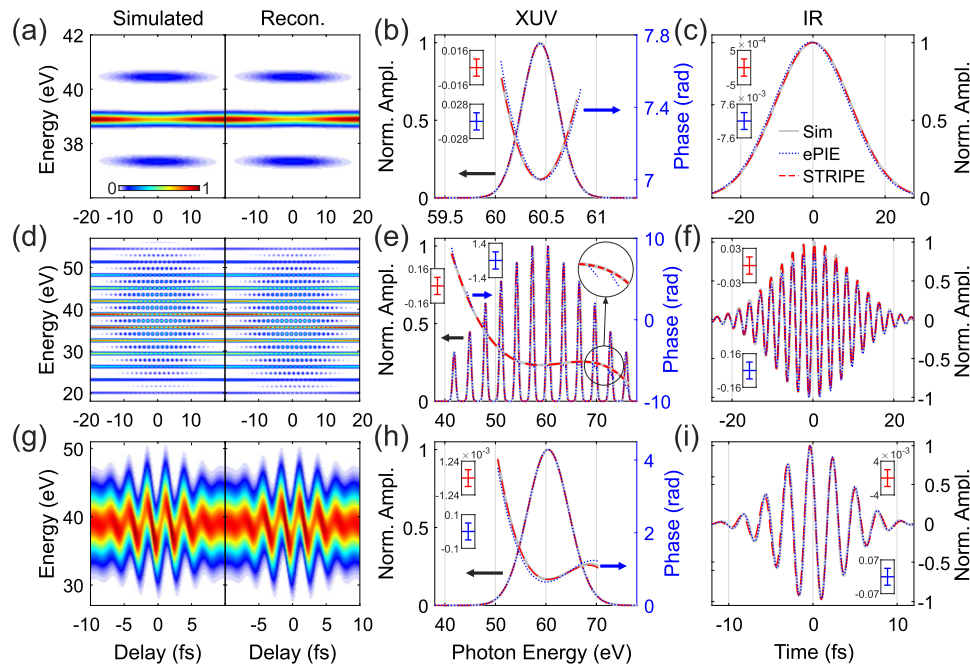


**FIG. 3.** The left panels of the first column display the spectrograms simulated with the SFA model of Eq. (1) for the case of a single harmonic [SH, (a)], an attosecond pulse train [APT, (d)], and an isolated attosecond pulse [IAP, (g)]. The STRIPE reconstructed spectrograms for each case are reported on the right side of the same figures. The second column [panels (b), (e), and (h)] shows the simulated (solid gray), the ePIE (blue dotted), and the STRIPE (red dashed) retrieved XUV pulses in spectral amplitude and phase. With the same color coding, the IR pulses, simulated or reconstructed with ePIE and STRIPE, are reported in the last column on the right [panels (c), (f), and (i)]. Due to the loss of temporal resolution, only the IR envelope is shown in the SH case. In all panels, the insets display a representative error bar calculated as twice the standard deviation over several reconstructions performed by varying the initial guess both for STRIPE (red) and ePIE (blue). Only the spectral phase of the XUV radiation is reconstructed with STRIPE. In the related panels, the presented error bars thus refer to the spectral phase both for STRIPE and ePIE in order to allow a direct comparison.

06 July 2023 07:08:36

## B. Noisy and imperfect traces

The simplicity and flexibility of STRIPE allow for its application to cases that cannot be treated with standard algorithms, e.g., extremely noisy traces. Figure 4(a) shows the spectrogram,  $S(\omega, \tau)$ , generated by a double attosecond pulse with non-trivial spectral phase [gray curves in Fig. 4(e)] and an  $\sim 8$  fs IR pulse [gray curve in Fig. 4(f)]. To simulate a realistic experiment, we added noise with a white component, a component proportional to the signal strength, and a  $1/f$  component in lab time. Experimentally, this latter phenomenon originates mainly from the instabilities of the laser parameters. The rather low resulting signal-to-noise ratio (SNR = 1.5 where the signal is higher than 1%) prevents the correct reconstruction through standard algorithms. Even in the case of ePIE, characterized by relatively high robustness against noise,<sup>37,48</sup> the retrieved IR and XUV pulses [blue-dotted curves in Figs. 3(e) and 3(f)], significantly deviate from the exact solution.

Figure 4(b) reports the related IR-off spectrogram,  $S_0(\omega, \tau)$ , obtained by simulating an XUV-only photoelectron spectrum at each delay immediately after the acquisition of a two-color spectrum as it would be done in a real pump-on/pump-off acquisition scheme. As the low-frequency component of the noise is almost identical in the two spectrograms, the differential trace  $\Delta S = S(\omega, \tau) - S_0(\omega, \tau)$

[Fig. 4(c)] inherently exhibits a lower noise content. Due to its versatility, STRIPE can be modified to run on the differential trace, in contrast to standard algorithms, greatly increasing the overall robustness against noise. In this case, the moduli of the IR and XUV spectra,  $|\hat{E}(\omega)|$  and  $|\hat{E}_x(\omega)|$ , are fixed to the experimental ones, e.g., measured independently with a spectrometer. The algorithm updates only the spectral phases, fitting directly  $\Delta S(\omega, \tau)$ . We found this approach particularly useful with non-ideal traces for two main reasons: (i) as the measurement of the photon spectrum is usually way more accurate than the detection of the photoelectron spectrum, this procedure delivers self-consistent reconstructions and allows us to account for acquisition artifacts; (ii) in this implementation, the algorithm updates only the spectral phases, fitting directly  $\Delta S(\omega, \tau)$ , which is inherently more robust against noise. The result is shown in Fig. 4(d), and the reconstructed XUV and IR pulses are reported in Figs. 4(e) and 4(f) by the red-dashed curves. Both quantities are retrieved with high accuracy despite the extreme noise level, whereas the ePIE reconstruction cannot properly retrieve the spectro-temporal characteristics of the pulses. Despite being relatively robust against noise [proven to perform better than the principal components generalized projections algorithm (PCGPA) and the least squares generalized projections algorithm (LSGPA)<sup>37</sup>,

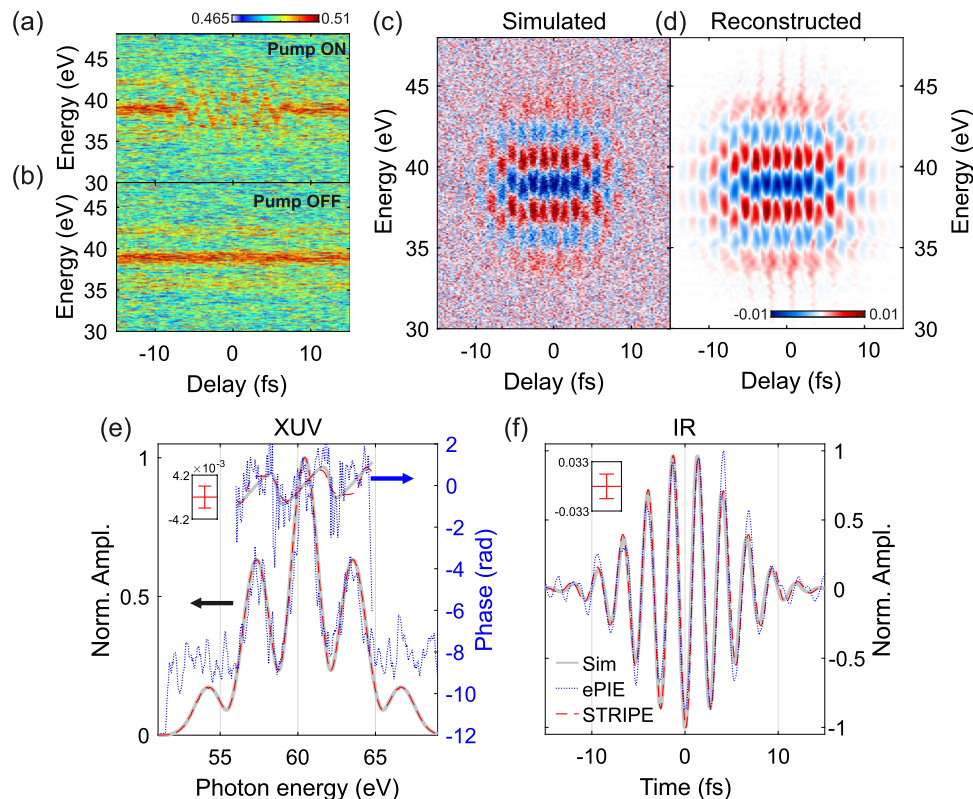


**FIG. 4.** Simulated pump-on (a) and pump-off (b) acquisition of a noisy photoelectron trace. (c) Resulting differential photoelectron trace obtained by performing the difference between the data in (a) and (b). (d) STRIPE reconstruction of the differential trace. (e) Simulated (gray), ePIE (dotted blue), and STRIPE (dashed red) reconstructed XUV spectral amplitude and phase. (f) Simulated, ePIE and STRIPE reconstructions of the IR pulse [same color coding as in (e)]. In panels (e) and (f), the insets display the maximum error bar calculated as twice the standard deviation over several STRIPE reconstructions with different initial guesses.

ePIE interprets any feature in the spectrogram as real, seriously challenging the code convergence<sup>49</sup> and leading to a spectrally broader and noisy reconstructed XUV pulse [Fig. 4(e)]. STRIPE, instead, exhibits a stronger rejection of noise, achieved by performing the retrieval on the differential spectrogram. Indeed, the simple operation of collecting IR-off spectra and computing the differential trace already has the effect of reducing the noise level significantly, as seen from Figs. 4(a)–4(c). Finally, STRIPE is based on a nonlinear fitting procedure that uses semi-analytical functions, and this naturally leads to high robustness with respect to residual noise, as any unphysical feature in the differential spectrogram that cannot be described by the underlying mathematical model is intrinsically rejected.

The capability to account for additional physical constraints enhances the convergence speed and allows treating other experimental non-idealities directly during reconstruction. A remarkable example is the finite IRF of the electron acquisition system. While the energy resolution of a typical TOF spectrometer in the XUV spectral region is on the order of tens of meVs,<sup>50</sup> the overall response of the electronic acquisition system and spatial average in the

interaction geometry<sup>51</sup> can reduce the effective resolution to hundreds of meVs.<sup>40</sup> Even if this is normally sufficient to properly collect broad spectra such as the ones generated by IAPs, it can prevent the correct acquisition of narrow spectra (i.e., SH ionization) or in the presence of sharp spectral features (e.g., ionization by APTs).

Figure 5(a) shows the simulated photoelectron spectrum obtained by ionizing Ne with harmonic 39 (intensity FWHM duration of 4 fs and central energy of about 60.5 eV) and acquired with a Gaussian IRF having an FWHM of 250 meV (orange curve in the inset). Due to the IRF, the electron spectrum (green curve) is significantly broader than the photon spectrum (black curve). As a result, standard reconstruction algorithms, which assume the two spectra to be identical, will predict a significantly shorter XUV pulse of about 3 fs duration [compare the ePIE reconstruction, blue-dotted curve, with the exact solution, gray solid curve, in Fig. 5(d)]. It is worth noticing that the deconvolution problem is ill-posed.<sup>52</sup> Therefore, it is not always possible to remove the effect of the IRF by deconvoluting the reconstruction results. If the IRF can be reasonably modeled, STRIPE allows for solving this issue by running the algorithm over the raw differential trace [Fig. 4(b)] while fixing the

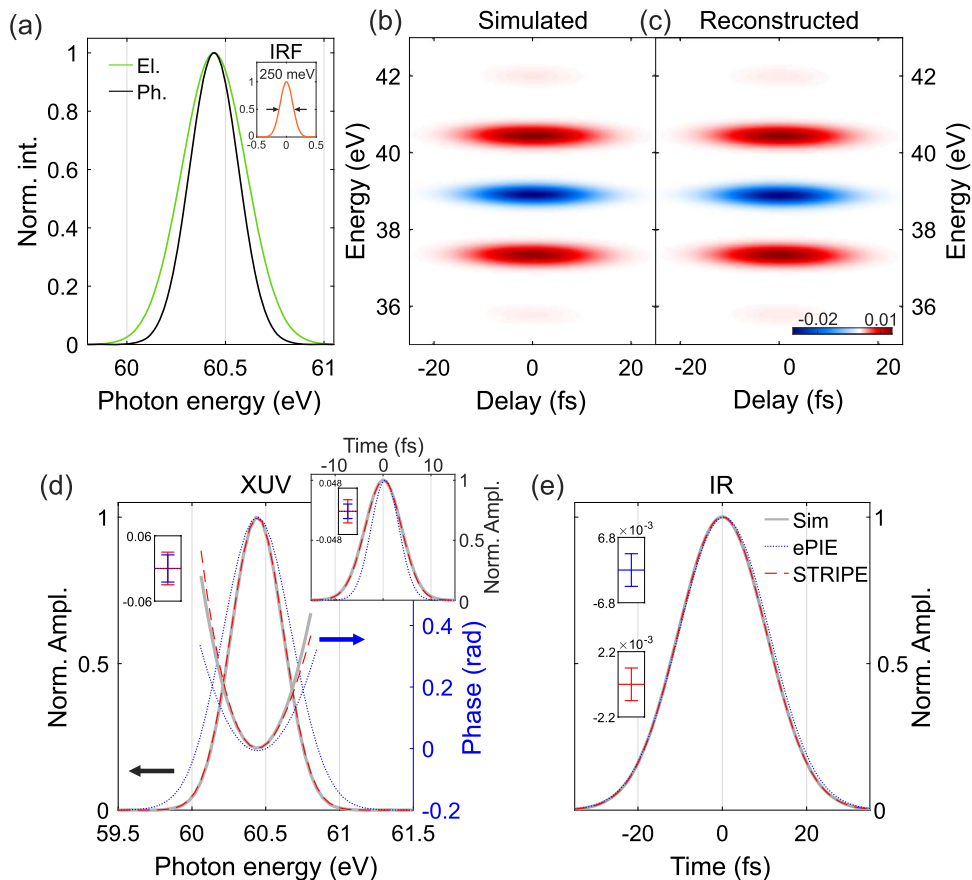


**FIG. 5.** (a) Comparison between the photon spectrum of a single harmonic (black curve) and the associated photoelectron spectrum shifted by the Ne ionization potential (green curve), obtained in the case of a non-instantaneous IRF (orange curve in the inset). (b) and (c) Simulated and STRIPE reconstructed differential trace. (d) Simulated (gray), ePIE (dotted blue), and STRIPE (dashed red) reconstructed XUV spectral amplitude and phase. The inset shows the associated XUV temporal profile. (e) Simulated, ePIE and STRIPE reconstructions of the IR pulse [same color coding as in (d)]. In panels (d) and (e), the insets display the maximum error bar calculated as twice the standard deviation over several STRIPE (red) and ePIE (blue) reconstructions with different initial guesses.



actual XUV photon spectrum. At each iteration, the calculated  $\Delta S$  is convoluted by the IRF before being compared with the input so that its effect is directly included in the reconstruction. The result is shown in Fig. 5(c), and the associated XUV and IR pulses are reported in Figs. 5(d) and 5(e) (red-dashed curves). STRIPE perfectly retrieves the actual pulses, despite the significant distortion introduced by the IRF. It is worth noticing that, in principle, one could apply a similar scheme and include the IRF in standard reconstruction algorithms. However, the additional convolution operation repeated at each iteration may significantly alter the functioning of a traditional ePIE implementation, where the way IR and XUV are updated makes them strongly interlaced. An abrupt change in the retrieved XUV spectrum during the iterations, as induced by the required convolution step, would need careful implementation and could seriously hinder convergence. This problem is circumvented in STRIPE due to the higher flexibility of its mathematical model, which allows one to directly implement an additional constraint as the IRF for the XUV spectrum.

### V. APPLICATION TO EXPERIMENTAL TRACES

The results presented in the previous sections prove STRIPE to be a valuable tool for pulse characterization, with accuracy at least comparable to that of other available reconstruction algorithms yet with increased versatility and robustness. However, a good reconstruction method is of broad interest if it is proven to be applicable to both simulated and experimental data.

The first column on the left in Figs. 6(a), 6(e), and 6(i) (left side) shows the experimental  $\Delta S(\omega, \tau)$  obtained by ionizing Ne with an SH (top row, 23rd harmonic selected by a time-delay compensated monochromator<sup>53</sup>), and APT (middle row), and an IAP (bottom row). The IR intensity used with the SH is  $2.5 \times 10^{11} \text{ W/cm}^2$ , while with the APT and IAP, the intensity was set to 1.1 and  $3 \times 10^{12} \text{ W/cm}^2$ , respectively. The differential spectrograms reconstructed with STRIPE are reported on the right side of the same column [Figs. 6(a), 6(e), and 6(i), right side]. In all cases, the XUV spectra are fixed to the ones independently obtained with photon

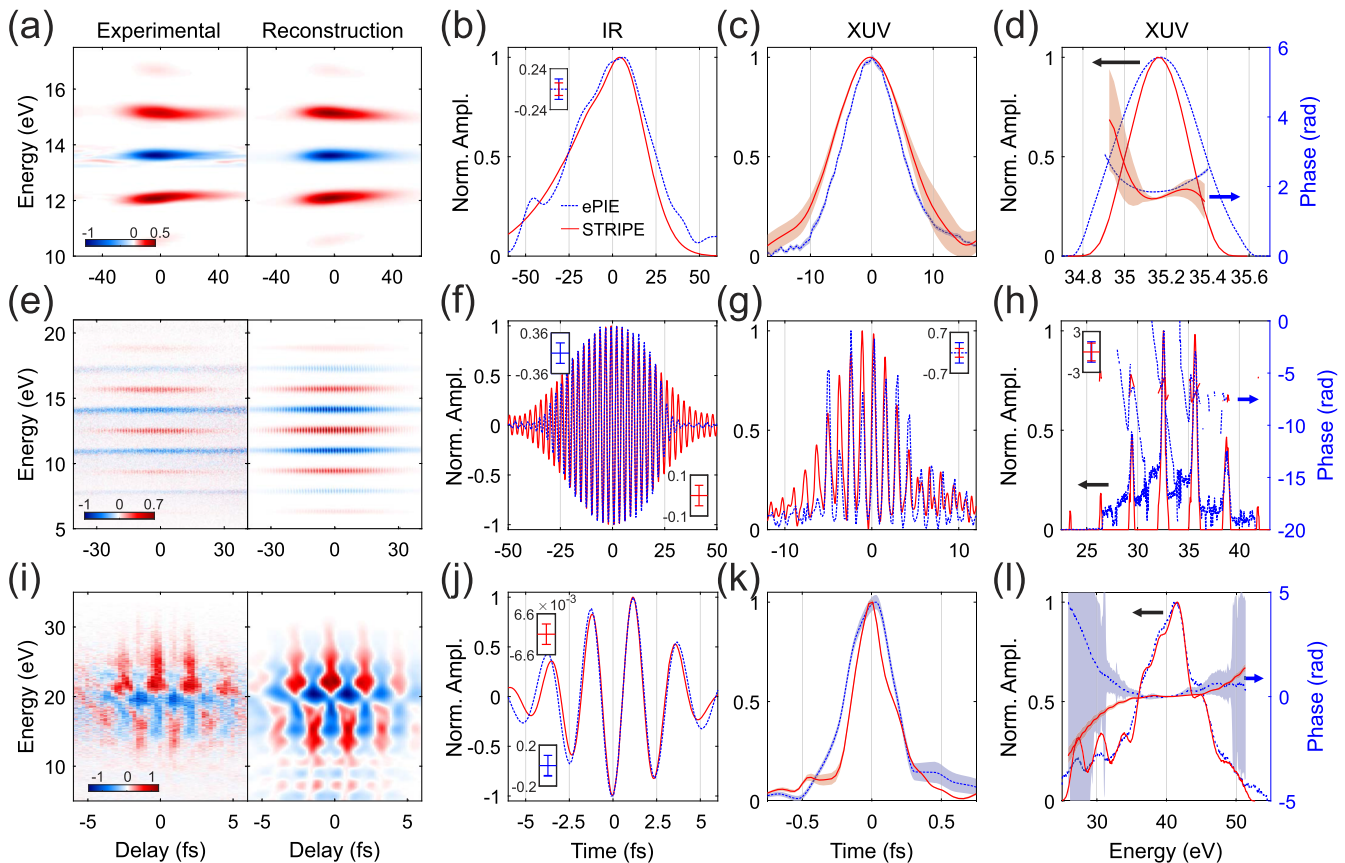


**FIG. 6.** The left panels in the first column [panels (a), (e), and (i), left side] display the experimental differential spectrograms obtained in Ne with a SH (a), an APT (e), and an IAP (i). The STRIPE reconstructions for each case are reported on the right side of the same figures. The second [panels (b), (f), and (j)] and third [panels (c), (g), and (k)] columns show the ePIE (blue dotted) and STRIPE (red solid) retrieved IR and XUV temporal profiles, respectively. With the same color coding, the XUV spectral amplitude and phase are reported in the last column on the right [panels (d), (h), and (l)]. Due to the loss of temporal resolution, only the IR envelope is shown in the SH case. In all panels, the shaded area represents twice the standard deviation over several STRIPE (red) and ePIE (blue) reconstructions with different initial guesses. If the error was too small or impossible to read on the plot, the maximum standard deviation is reported in a separate inset (red for STRIPE, blue for ePIE).

06 July 2023 07:08:36

spectrometers, and the experimental IRF is accounted for. The retrieved temporal profiles of the IR and XUV pulses are shown in the second [Figs. 6(b), 6(f), and 6(j)] and third [Figs. 6(c), 6(g), and 6(k)] columns, respectively. The last column on the right displays the XUV spectral amplitude and phase [Figs. 6(d), 6(h), and 6(l)]. In all these panels, the STRIPE outcome (red solid curves) is compared to the ePIE reconstruction (blue dotted curves).

While STRIPE and ePIE results qualitatively agree in all cases, the advantages of our method become evident in the cases of SH and APT, where ePIE fails to perfectly reproduce the photon spectrum (identical to the red curve in the last column on the right), thus predicting a shorter harmonic pulse [Fig. 6(c)] and underestimating the relative strength of the pulses in the APT [Fig. 6(g)]. Indeed, the temporal profile of the APT reconstructed by ePIE shows a nonphysical modulation of the pulse amplitudes, where one pulse every two in the train is amplified. This effect originates from finite IRF and the non-zero photoelectron counts between two consecutive harmonic peaks, which are interpreted as real by ePIE. Moreover, this also deeply affects the IR pulse reconstruction, shortening its duration [Fig. 6(g)]. Finally, for the case of the IAP, ePIE and STRIPE reconstructions largely agree despite the use of a short and intense IR pulse, which seriously challenges the applicability of our algorithm.

The results of Figs. 6(d) and 6(l) seem to suggest that STRIPE retrieves a stronger TOD if compared to ePIE. We note that this is accidental and not linked to an inherent difference in the sensitivity of STRIPE to higher spectral dispersion orders. Indeed, the simulations reported in Fig. 3 show that both methods are capable of reconstructing non-flat spectral phases. The qualitatively different phases retrieved with the experimental data can be explained by considering that the two algorithms also retrieve appreciably different spectral amplitudes.

It is important to stress that the experimental data in Fig. 6 has not been manipulated before reconstruction. While it is true that post-processing data optimization may improve the ePIE results, one needs to be aware that any manipulation of experimental data inevitably includes a certain degree of arbitrariness, for instance, the operations of background removal or noise filtering. In this regard, the goal of our investigation is to introduce a new reconstruction algorithm that can run over raw experimental data, substantially reducing this degree of arbitrariness to a minimum, if not to zero.

## VI. CONCLUSIONS

In this work, we have introduced a new approach called STRIPE for the reconstruction of attosecond and femtosecond pulses from two-color photoelectron spectrograms. At first, the method was tested against simulated data and compared to standard FROG-like algorithms, revealing comparable accuracy with significantly reduced computational costs. Moreover, the higher flexibility of STRIPE allows it to be run on differential traces, imposing the radiation spectra to match the experimental ones and including a finite IRF of the detection system. This strongly enhances the code's convergence and robustness against noise, allowing for the reconstruction of extremely noisy or distorted traces where standard approaches fail. Finally, we applied STRIPE to experimental traces, proving it to be capable of successfully reconstructing XUV pulses ranging from a few-fs pulse to an attosecond pulse train

or an isolated attosecond pulse. The availability of a fast, versatile, and reliable method for ultrashort pulse characterization opens the way to the characterization of novel advanced light sources and low signal-to-noise traces, which are of key importance for a wide class of time-resolved experiments that strongly depend on the accuracy of the determination of the temporal properties of the light pulses.

## ACKNOWLEDGMENTS

This project has received funding from the European Research Council (ERC) under the European Union's Horizon 2020 research and innovation program (Grant Agreement No. 848411, title AuDACE; Grant Agreement No. 951224, title TOMATTO); and Laserlab-Europe EU-H2020 GA under Grant No. 871124. M.L. and G.I. further acknowledge funding from MIUR PRIN aSTAR, Grant No. 2017RKWTMY. M.N. acknowledges funding from MIUR PRIN, Grant No. 20173B72NB. R.B.-V. acknowledges funding from the Fondazione Cariplo (Grant No. 2020-4380, DINAMO). F.M. acknowledges the POLIMI SOE fellowship.

## AUTHOR DECLARATIONS

### Conflict of Interest

The authors have no conflicts to disclose.

### Author Contributions

G.L.D. and G.I. contributed equally to this work.

**Gian Luca Dolso:** Formal analysis (lead); Investigation (lead); Methodology (supporting); Software (equal); Writing – original draft (supporting); Writing – review & editing (equal). **Giacomo Inzani:** Formal analysis (supporting); Investigation (lead); Methodology (lead); Software (equal); Writing – review & editing (equal). **Nicola Di Palo:** Formal analysis (supporting); Investigation (lead); Methodology (supporting); Project administration (supporting); Supervision (equal); Writing – original draft (supporting); Writing – review & editing (equal). **Bruno Moio:** Conceptualization (equal); Investigation (supporting). **Fabio Medeghini:** Investigation (supporting). **Rocío Borrego-Varillas:** Supervision (equal); Writing – review & editing (equal). **Mauro Nisoli:** Supervision (equal); Writing – review & editing (equal). **Matteo Lucchini:** Conceptualization (equal); Funding acquisition (lead); Project administration (lead); Supervision (equal); Writing – original draft (lead); Writing – review & editing (equal).

## DATA AVAILABILITY

The data that support the findings of this study are available from the corresponding author upon reasonable request.

## REFERENCES

- 1R. Borrego-Varillas, M. Lucchini, and M. Nisoli, "Attosecond spectroscopy for the investigation of ultrafast dynamics in atomic, molecular and solid-state physics," *Rep. Prog. Phys.* **85**, 066401 (2022).

- <sup>2</sup>M. Nisoli, P. Decleva, F. Calegari, A. Palacios, and F. Martín, “Attosecond electron dynamics in molecules,” *Chem. Rev.* **117**, 10760–10825 (2017).
- <sup>3</sup>M. Isinger, R. J. Squibb, D. Busto, S. Zhong, A. Harth, D. Kroon, S. Nandi, C. L. Arnold, M. Miranda, J. M. Dahlström, E. Lindroth, R. Feifel, M. Gisselbrecht, and A. L’Huillier, “Photoionization in the time and frequency domain,” *Science* **358**, 893–896 (2017).
- <sup>4</sup>M. Ossiander, F. Siegrist, V. Shirvanyan, R. Pazourek, A. Sommer, T. Latka, A. Guggenmos, S. Nagele, J. Feist, J. Burgdörfer, R. Kienberger, and M. Schultze, “Attosecond correlation dynamics,” *Nat. Phys.* **13**, 280–285 (2017).
- <sup>5</sup>C. Cirelli, C. Marante, S. Heuser, C. L. M. Petersson, Á. J. Galán, L. Argenti, S. Zhong, D. Busto, M. Isinger, S. Nandi, S. Maclot, L. Rading, P. Johnsson, M. Gisselbrecht, M. Lucchini, L. Gallmann, J. M. Dahlström, E. Lindroth, A. L’Huillier, F. Martín, and U. Keller, “Anisotropic photoemission time delays close to a Fano resonance,” *Nat. Commun.* **9**, 955 (2018).
- <sup>6</sup>F. Calegari, D. Ayuso, A. Trabattoni, L. Belshaw, S. De Camillis, S. Anumula, F. Frassetto, L. Poletto, A. Palacios, P. Decleva, J. B. Greenwood, F. Martín, and M. Nisoli, “Ultrafast electron dynamics in phenylalanine initiated by attosecond pulses,” *Science* **346**, 336–339 (2014).
- <sup>7</sup>Y. Kobayashi, K. F. Chang, T. Zeng, D. M. Neumark, and S. R. Leone, “Direct mapping of curve-crossing dynamics in IBR by attosecond transient absorption spectroscopy,” *Science* **365**, 79–83 (2019).
- <sup>8</sup>S. Biswas, B. Förg, L. Ortman, J. Schötz, W. Schweinberger, T. Zimmermann, L. Pi, D. Baykusheva, H. A. Masood, I. Lontos, A. M. Kamal, N. G. Kling, A. F. Alharbi, M. Alharbi, A. M. Azzeer, G. Hartmann, H. J. Wörner, A. S. Landsman, and M. F. Kling, “Probing molecular environment through photoemission delays,” *Nat. Phys.* **16**, 778–783 (2020).
- <sup>9</sup>I. Jordan, M. Huppert, D. Rattenbacher, M. Peper, D. Jelovina, C. Perry, A. von Conta, A. Schild, and H. J. Wörner, “Attosecond spectroscopy of liquid water,” *Science* **369**, 974–979 (2020).
- <sup>10</sup>X. Gong, S. Heck, D. Jelovina, C. Perry, K. Zinchenko, R. Lucchese, and H. J. Wörner, “Attosecond spectroscopy of size-resolved water clusters,” *Nature* **609**, 507–511 (2022).
- <sup>11</sup>Z. Tao, C. Chen, T. Szilvási, M. Keller, M. Mavrikakis, H. Kapteyn, and M. Murnane, “Direct time-domain observation of attosecond final-state lifetimes in photoemission from solids,” *Science* **353**, 62–67 (2016).
- <sup>12</sup>L. Kasmi, M. Lucchini, L. Castiglioni, P. Kliuiev, J. Osterwalder, M. Hengsberger, L. Gallmann, P. Krüger, and U. Keller, “Effective mass effect in attosecond electron transport,” *Optica* **4**, 1492 (2017).
- <sup>13</sup>S. Heinrich, T. Saule, M. Högner, Y. Cui, V. S. Yakovlev, I. Pupeza, and U. Kleineberg, “Attosecond intra-valence band dynamics and resonant-photoemission delays in W(110),” *Nat. Commun.* **12**, 3404 (2021).
- <sup>14</sup>M. Schultze, E. M. Bothschafter, A. Sommer, S. Holzner, W. Schweinberger, M. Fiess, M. Hofstetter, R. Kienberger, V. Apalkov, V. S. Yakovlev, M. I. Stockman, and F. Krausz, “Controlling dielectrics with the electric field of light,” *Nature* **493**, 75–78 (2013).
- <sup>15</sup>H. Mashiko, Y. Chisuga, I. Katayama, K. Oguri, H. Masuda, J. Takeda, and H. Gotoh, “Multi-petahertz electron interference in Cr:Al<sub>2</sub>O<sub>3</sub> solid-state material,” *Nat. Commun.* **9**, 1468 (2018).
- <sup>16</sup>M. Lucchini, S. A. Sato, G. D. Lucarelli, B. Moio, G. Inzani, R. Borrego-Varillas, F. Frassetto, L. Poletto, H. Hübener, U. De Giovannini, A. Rubio, and M. Nisoli, “Unravelling the intertwined atomic and bulk nature of localised excitons by attosecond spectroscopy,” *Nat. Commun.* **12**, 1021 (2021).
- <sup>17</sup>J. Itatani, F. Quéré, G. L. Yudin, M. Y. Ivanov, F. Krausz, and P. B. Corkum, “Attosecond streak camera,” *Phys. Rev. Lett.* **88**, 173903 (2002).
- <sup>18</sup>Y. Mairesse and F. Quéré, “Frequency-resolved optical gating for complete reconstruction of attosecond bursts,” *Phys. Rev. A* **71**, 011401 (2005).
- <sup>19</sup>S. Hu, M. Hartmann, A. Harth, C. Ott, and T. Pfeifer, “Noise effects and the impact of detector responses on the characterization of extreme ultraviolet attosecond pulses,” *Appl. Opt.* **59**, 2121–2127 (2020).
- <sup>20</sup>Z. Zhu, J. White, Z. Chang, and S. Pang, “Attosecond pulse retrieval from noisy streaking traces with conditional variational generative network,” *Sci. Rep.* **10**, 5782 (2020).
- <sup>21</sup>X. Zhao, S.-J. Wang, W.-W. Yu, H. Wei, C. Wei, B. Wang, J. Chen, and C. D. Lin, “Metrology of time-domain soft x-ray attosecond pulses and reevaluation of pulse durations of three recent experiments,” *Phys. Rev. Appl.* **13**, 034043 (2020).
- <sup>22</sup>G. Laurent, W. Cao, H. Li, Z. Wang, I. Ben-Itzhak, and C. L. Cocke, “Attosecond control of orbital parity mix interferences and the relative phase of even and odd harmonics in an attosecond pulse train,” *Phys. Rev. Lett.* **109**, 083001 (2012).
- <sup>23</sup>P. D. Keathley, S. Bhardwaj, J. Moses, G. Laurent, and F. X. Kärtner, “Volkov transform generalized projection algorithm for attosecond pulse characterization,” *New J. Phys.* **18**, 073009 (2016).
- <sup>24</sup>X. Zhao, H. Wei, Y. Wu, and C. D. Lin, “Phase-retrieval algorithm for the characterization of broadband single attosecond pulses,” *Phys. Rev. A* **95**, 043407 (2017).
- <sup>25</sup>J. White and Z. Chang, “Attosecond streaking phase retrieval with neural network,” *Opt. Express* **27**, 4799 (2019).
- <sup>26</sup>W.-W. Yu, X. Zhao, H. Wei, S.-J. Wang, and C. D. Lin, “Method for spectral phase retrieval of single attosecond pulses utilizing the autocorrelation of photoelectron streaking spectra,” *Phys. Rev. A* **99**, 033403 (2019).
- <sup>27</sup>C. Bourassin-Bouchet, L. Barreau, V. Gruson, J.-F. Hergott, F. Quéré, P. Salières, and T. Ruchon, “Quantifying decoherence in attosecond metrology,” *Phys. Rev. X* **10**, 031048 (2020).
- <sup>28</sup>P. Tzallas, D. Charalambidis, N. A. Papadogiannis, K. Witte, and G. D. Tsakiris, “Direct observation of attosecond light bunching,” *Nature* **426**, 267–271 (2003).
- <sup>29</sup>K. T. Kim, C. Zhang, A. D. Shiner, S. E. Kirkwood, E. Frumker, G. Gariepy, A. Naumov, D. M. Villeneuve, and P. B. Corkum, “Manipulation of quantum paths for space-time characterization of attosecond pulses,” *Nat. Phys.* **9**, 159–163 (2013).
- <sup>30</sup>S. Li, Z. Guo, R. N. Coffee, K. Hegazy, Z. Huang, A. Natan, T. Osipov, D. Ray, A. Marinelli, and J. P. Cryan, “Characterizing isolated attosecond pulses with angular streaking,” *Opt. Express* **26**, 4531 (2018).
- <sup>31</sup>O. Pedatzur, A. Trabattoni, B. Leshem, H. Shalmoni, M. C. Castrovilli, M. Galli, M. Lucchini, E. Månsson, F. Frassetto, L. Poletto, B. Nadler, O. Raz, M. Nisoli, F. Calegari, D. Oron, and N. Dudovich, “Double-blind holography of attosecond pulses,” *Nat. Photonics* **13**, 91–95 (2019).
- <sup>32</sup>M. Lucchini, G. D. Lucarelli, M. Murari, A. Trabattoni, N. Fabris, F. Frassetto, S. De Silvestri, L. Poletto, and M. Nisoli, “Few-femtosecond extreme-ultraviolet pulses fully reconstructed by a ptychographic technique,” *Opt. Express* **26**, 6771–6784 (2018).
- <sup>33</sup>D. E. Rivas, S. Serkez, T. M. Baumann, R. Boll, M. K. Czwalińska, S. Dold, A. de Fanis, N. Gerasimova, P. Grychtol, B. Lautenschlager, M. Lederer, T. Jezynski, D. Kane, T. Mazza, J. Meier, J. Müller, F. Pallas, D. Rompotis, P. Schmidt, S. Schulz, S. Usenko, S. Venkatesan, J. Wang, and M. Meyer, “High-temporal-resolution X-ray spectroscopy with free-electron and optical lasers,” *Optica* **9**, 429–430 (2022).
- <sup>34</sup>T. Gaumnitz, A. Jain, and H. J. Wörner, “Complete reconstruction of ultra-broadband isolated attosecond pulses including partial averaging over the angular distribution,” *Opt. Express* **26**, 14719 (2018).
- <sup>35</sup>C. Bourassin-Bouchet and M.-E. Couprie, “Partially coherent ultrafast spectrography,” *Nat. Commun.* **6**, 6465 (2015).
- <sup>36</sup>L. Pedrelli, P. D. Keathley, L. Cattaneo, F. X. Kärtner, and U. Keller, “Complete phase retrieval of photoelectron wavepackets,” *New J. Phys.* **22**, 053028 (2020).
- <sup>37</sup>M. Lucchini, M. H. Brüggemann, A. Ludwig, L. Gallmann, U. Keller, and T. Feurer, “Ptychographic reconstruction of attosecond pulses,” *Opt. Express* **23**, 29502 (2015).
- <sup>38</sup>R. Borrego-Varillas and M. Lucchini, “Reconstruction of atomic resonances with attosecond streaking,” *Opt. Express* **29**, 9711–9722 (2021).
- <sup>39</sup>L. B. Madsen, “Strong-field approximation in laser-assisted dynamics,” *Am. J. Phys.* **73**, 57–62 (2005).
- <sup>40</sup>M. Lucchini, F. Medeghini, Y. Wu, F. Vismarra, R. Borrego-Varillas, A. Crego, F. Frassetto, L. Poletto, S. A. Sato, H. Hübener, U. De Giovannini, Á. Rubio, and M. Nisoli, “Controlling Floquet states on ultrashort time scales,” *Nat. Commun.* **13**, 7103 (2022).
- <sup>41</sup>M. Kitzler, N. Milosevic, A. Scrinzi, F. Krausz, and T. Brabec, “Quantum theory of attosecond XUV pulse measurement by laser dressed photoionization,” *Phys. Rev. Lett.* **88**, 173904 (2002).
- <sup>42</sup>D. J. Kane, “Recent progress toward real-time measurement of ultrashort laser pulses,” *IEEE J. Quantum Electron.* **35**, 421–431 (1999).

- <sup>43</sup>J. Gagnon, E. Goulielmakis, and V. S. Yakovlev, "The accurate FROG characterization of attosecond pulses from streaking measurements," *Appl. Phys. B* **92**, 25–32 (2008).
- <sup>44</sup>B. Moio, G. L. Dolso, G. Inzani, N. Di Palo, R. Borrego-Varillas, M. Nisoli, and M. Lucchini, "Time-frequency mapping of two-colour photoemission driven by harmonic radiation," *J. Phys. B: At., Mol. Opt. Phys.* **54**, 154003 (2021).
- <sup>45</sup>M. Chini, S. Gilbertson, S. D. Khan, and Z. Chang, "Characterizing ultrabroadband attosecond lasers," *Opt. Express* **18**, 13006–13016 (2010).
- <sup>46</sup>G. Laurent, W. Cao, I. Ben-Itzhak, and C. L. Cocke, "Attosecond pulse characterization," *Opt. Express* **21**, 16914–16927 (2013).
- <sup>47</sup>H. Wei, A.-T. Le, T. Morishita, C. Yu, and C. D. Lin, "Benchmarking accurate spectral phase retrieval of single attosecond pulses," *Phys. Rev. A* **91**, 023407 (2015).
- <sup>48</sup>M. Murari, G. D. Lucarelli, M. Lucchini, and M. Nisoli, "Robustness of the ePIE algorithm for the complete characterization of femtosecond, extreme ultra-violet pulses," *Opt. Express* **28**, 10210 (2020).
- <sup>49</sup>H. Wang, M. Chini, S. D. Khan, S. Chen, S. Gilbertson, X. Feng, H. Mashiko, and Z. Chang, "Practical issues of retrieving isolated attosecond pulses," *J. Phys. B: At., Mol. Opt. Phys.* **42**, 134007 (2009).
- <sup>50</sup>G. D. Lucarelli, B. Moio, G. Inzani, N. Fabris, L. Moscardi, F. Frassetto, L. Poletto, M. Nisoli, and M. Lucchini, "Novel beamline for attosecond transient reflection spectroscopy in a sequential two-foci geometry," *Rev. Sci. Instrum.* **91**, 053002 (2020).
- <sup>51</sup>F. Vismarra, R. Borrego-Varillas, Y. Wu, D. Mocchi, M. Nisoli, and M. Lucchini, "Ensemble effects on the reconstruction of attosecond pulses and photoemission time delays," *J. Phys.: Photonics* **4**, 034006 (2022).
- <sup>52</sup>S. M. Riad, "The deconvolution problem: An overview," *Proc. IEEE* **74**, 82–85 (1986).
- <sup>53</sup>L. Poletto, P. Villoresi, F. Frassetto, F. Calegari, F. Ferrari, M. Lucchini, G. Sansone, and M. Nisoli, "Time-delay compensated monochromator for the spectral selection of extreme-ultraviolet high-order laser harmonics," *Rev. Sci. Instrum.* **80**, 123109 (2009).